

Plane harmonic waves in fractional orthotropic magneto-thermoelastic solid with rotation and two-temperature

Himanshi^a and Parveen Lata*

Department of Mathematics, Punjabi University, Patiala, Punjab, India

(Received November 30, 2022, Revised February 22, 2023, Accepted March 20, 2023)

Abstract. The present research is focused on the study of plane harmonic waves in a two-dimensional orthotropic magneto-thermoelastic media with fractional order theory of generalized thermoelasticity in the light of two-temperature and rotation due to time harmonic sources. Here, we studied three types of waves namely quasi-longitudinal (QL), quasi-transverse (QTS) and quasi thermal (QT) waves. The variations in the wave properties such as phase velocity, attenuation coefficient and specific loss have been noticed with respect to frequency for the reflected waves. Further the value of amplitude ratios, energy ratios and penetration depth are computed numerically with respect to angle of incidence. The numerical simulated results are presented graphically to show the effect of fractional parameter based on its conductivity ($0 < \alpha < 1$ for weak, $\alpha = 1$ for normal, $1 < \alpha \leq 2$ for strong conductivity) on all the components.

Keywords: amplitude ratios; attenuation coefficient; energy ratios; fractional order; frequency; harmonic plane waves; orthotropic medium; penetration depth; phase velocity; rotation; specific loss; three-phase lags

1. Introduction

A lot of research work has been carried out in the area of thermoelastic surface waves. The study of harmonic plane waves in different media or interfaces is one of the interesting fields in scientific technology. These wave travel along the different interfaces and layers through the earth. Moreover, plane waves are special type of waves where the phase of a wave is constant over the plane which is perpendicular to the direction of wave propagation. Further, the study of plane waves in magneto-thermoelastic media has great importance in the solid mechanics due to its applications in the various fields like semiology, geophysics and earthquake engineering, nuclear fields, inspecting materials etc.

During the last few decades the wave propagation in anisotropic media has been widely studied. Chen and Gurtin (1968) and Chen *et al.* (1968, 1969) formulated two-temperature theory of thermoelasticity for deformable bodies. Heat conduction equation of this theory depends on two different types of temperatures thermodynamical temperature (T) and the conductive temperature

*Corresponding author, Associate Professor, E-mail: parveenlata@pbi.ac.in

^aPh.D. Scholar, E-mail: heena.zakhmi@gmail.com

(ϕ). The difference between these two temperatures is proportional to the heat supply. The two temperatures are equal in the absence of heat supply for time independent problems. For time dependent problems, the two temperatures are different regardless of the presence of heat supply. Moreover, fractional order theory came into existence during the second half of the 19th century and has been used to model polymer materials. The applications of fractional order theory are widely spread over the areas like in dynamics, fluid mechanics, biology, physics, mechanics of solids etc. Fractional order differential equations have been focus of many studies due to their non-localization property. Most of the problems of physical processes are solved with the help of fractional order heat conduction equations. The application of fractional calculus was first introduced by Abel to solve the tautochrone problem. Borejko (1996) studied the reflection and transmission coefficients for 3D plane waves in elastic media. Sinha and Elsibai (1997) analyzed the reflection and refraction of thermoelastic waves at an interface of two semi-infinite media with two relaxation times. Abd-Alla and Abbas (2002) examined the interactions in an infinite elastic cylinder placed in constant magnetic field and periodic load applied on its curved surface with the application of Lord Shulman and Green Lindsay theories of generalized thermoelasticity. Youssef (2006) formulated a new theory of generalized thermoelasticity by considering two-temperature generalized thermoelasticity theory for a homogeneous isotropic body without energy dissipation. Kaushal *et al.* (2010) studied the propagation of waves in generalized thermoelastic medium with two-temperature. Sharma and Bhargava (2014) studied the plane waves and fundamental solution in thermo-viscoelastic medium with voids.

Kumar and Gupta (2013) studied the plane wave propagation in anisotropic thermoelastic media with fractional order derivative and void. Zakaria (2014) examined the effect of hall current in a micropolar magneto-thermoelastic solid due to ramp type heat. Deswal and Kalkal (2014) studied the plane waves in a fractional order micropolar magneto-thermoelastic half-space. Das and Kanoria (2014) studied the finite thermal waves in a magneto-thermoelastic rotating medium. Sharma and Kumar (2013) studied the thermoelastic plane waves at an imperfect boundary of thermal conducting viscous liquid. Lata *et al.* (2016) studied the plane waves in transversely isotropic thermoelastic media with two-temperature and rotation. Marin *et al.* (2017) studied the qualitative results on mixed problem of micropolar bodies with microtemperatures. Abbas and Marin (2017) examined the analytical solution of thermoelastic interaction in a half space due to pulsed laser heating. Hobiny and Abbas (2017) studied the photothermal waves in an unbounded semiconductor medium with cylindrical cavity. Biswas and Abo-Dahab (2018) studied the effect of phase lags on Rayleigh wave propagation in initially stressed magneto-thermoelastic orthotropic medium. Othman *et al.* (2019a, 2019b) studied various plane wave problems in thermoelastic and magneto-thermoelastic media. Marin *et al.* (2019) extended of Dafermos's results for dynamical theory of inhomogeneous anisotropic bodies with a dipolar structure. Abouelregal *et al.* (2020) derived the fundamental equations in generalized thermoelastic diffusion with four lags and higher-order time-fractional derivatives. Ezzat (2020) studied the fractional thermo-viscoelastic response of biological tissue with variable thermal material properties. Lata and Himanshi (2021a, 2021b, 2021c) studied the various orthotropic thermoelastic problems in generalized thermoelasticity with fractional order heat transfer. Singh and Aarti (2021) studied the Reflection of plane waves from the boundary of a thermo-magneto-electroelastic solid half space. Djilali *et al.* (2021) studied the original four-variable quasi-3D shear deformation theory for the static and free vibration analysis of new type of sandwich plates with both FG face sheets and FGM hard core. Bouafia *et al.* (2021) analyzed the bending and free vibration characteristics of various compositions of FG plates on elastic foundation via quasi 3D HSDT model. Abbas *et al.* (2021)

studied the photo-thermal interactions in a semiconductor medium with a cylindrical cavity with two-temperature. Khamis *et al.* (2021) studied the effect of modified Ohm's and Fourier's laws on magneto thermo-viscoelastic waves with Green-Naghdi theory in a homogeneous isotropic hollow cylinder. Houari (2021) *et al.* studied the bending analysis of functionally graded plates using a new refined quasi 3D shear deformation theory and the concept of the neutral surface position. Merazka *et al.* (2021) studied the hygro-thermo-mechanical bending response of simply supported FG plates resting on elastic foundations. Bakoura *et al.* (2022) studied the mechanical behavior of composite plates by using simple three variable refined plate theory. Bhatti *et al.* (2022) analyzed the thermal and entropy generation of magnetic Eyring-Powell nanofluid containing silver and gold nano-particles with viscous dissipation in a wavy asymmetric channel. Bot *et al.* (2022) studied the effects of Pasternak foundation on the bending behavior of FG porous plates in hygrothermal environment. Djilali *et al.* (2022) analyzed the large cylindrical deflection of FG carbon nanotube-reinforced plates in thermal environment using a simple integral HSDT. Hebali *et al.* (2022) studied the effect of the variable visco-Pasternak foundations on the bending and dynamic behaviors of FG plates using integral HSDT model. Tahir *et al.* (2022) studied the effect of three-variable viscoelastic foundation on the wave propagation in functionally graded sandwich plates via a simple quasi-3D HSDT. Vinh *et al.* (2022) studied the static bending and buckling analysis of bi-directional functionally graded porous plates using an improved first-order shear deformation theory and FEM. Vinh and Tounsi studied the (2022) studied the free vibration analysis of functionally graded doubly curved nanoshells using nonlocal first-order shear deformation theory with variable nonlocal parameters. Zhang *et al.* (2022) examined the blood flow through anisotropically tapered arteries filled with magnetic zinc-oxide nanoparticles. Bhatti *et al.* (2023) studied the spectral relaxation computation of Maxwell fluid flow from a stretching surface with quadratic convection and non-Fourier heat flux using Lie symmetry transformations.

Including all the above discussed work, we conclude that the plane harmonic waves in an orthotropic magneto-thermoelastic medium in the context of fractional order heat transfer with combined effects of rotation and two-temperature has not been considered yet. So in the present research, we examined the effect of fractional order parameter on the plane wave properties in orthotropic media with and without energy dissipation in generalized thermoelasticity and noticed the variations in the values of all the field components with the help of graphs.

2. Basic equations

Following Lata *et al.* (2016), the simplified Maxwell's linear equation of electrodynamics for a slowly moving and perfectly conducting elastic solid are

$$\text{Curl } \vec{h} = \vec{j} + \varepsilon_0 \frac{\partial \vec{E}}{\partial t}, \quad (1)$$

$$\text{Curl } \vec{E} = -\mu_0 \frac{\partial \vec{h}}{\partial t}, \quad (2)$$

$$\vec{E} = -\mu_0 \left(\frac{\partial \vec{u}}{\partial t} \times H_0 \right), \quad (3)$$

$$\operatorname{div} \vec{h} = 0, \quad (4)$$

Maxwell stress components are given by

$$t_{ij} = \mu_0 (H_i h_j + h_j H_i - H_k h_k \delta_{ij}), \quad (5)$$

Where, t_{ij} is the Maxwell stress tensor, \vec{E} is the induced electric field vector, \vec{h} and \vec{H}_0 are the induced and external applied magnetic field vector, \vec{u} is the displacement vector, \vec{j} is the current density vector, ϵ_0 and μ_0 are the electric and magnetic permeabilities, δ_{ij} is the Kronecker delta respectively.

Following Lata and Himanshi (2021a), equation of motion for an orthotropic thermoelastic medium rotating uniformly with an angular velocity $\Omega = \Omega \vec{n}$, where \vec{n} is unit vector representing the direction of axis of rotation and taking into account Lorentz force is given by

$$\sigma_{ij,j} + F_i = \rho [\ddot{u}_i + (\Omega \times (\Omega \times \vec{u}))_i + (2 \Omega \times \dot{\vec{u}})_i], \quad (6)$$

Where, the components of Lorentz force are given by

$$F_i = \mu_0 (\vec{j} \times \vec{H}_0)_i, \quad (7)$$

Also, $\vec{H} = (0, H_0, 0)$, is the magnetic field strength, \vec{j} is the current density vector, μ_0 is the magnetic permeability. The additional terms $\Omega \times (\Omega \times \vec{u})$ and $2 \Omega \times \dot{\vec{u}}$ on the right side of above equation (6) are centripetal acceleration and Coriolis acceleration respectively.

Following Lata and Zakhmi (2020), heat equation in anisotropic medium with fractional order heat transfer and with three-phase-lags is given by

$$\begin{aligned} & K_{ij} \left(1 + \frac{\tau_t^\alpha}{\alpha!} \frac{\partial^\alpha}{\partial t^\alpha} \right) \phi_{,ji} + K_{ij}^* \left(1 + \frac{\tau_v^\alpha}{\alpha!} \frac{\partial^\alpha}{\partial t^\alpha} \right) \phi_{,ji} \\ & = \left(1 + \frac{\tau_q^\alpha}{\alpha!} \frac{\partial^\alpha}{\partial t^\alpha} + \frac{\tau_q^{2\alpha}}{2\alpha!} \frac{\partial^{2\alpha}}{\partial t^{2\alpha}} \right) (\rho C_E \ddot{T} + \beta_{ij} T_0 \ddot{e}_{ij}), \end{aligned} \quad (8)$$

Where,

$$\begin{aligned} \beta_{ij} &= c_{ijkl} \alpha_{kl}, \beta_{ij} = \beta_i \delta_{ij}, K_{ij} = K_i \delta_{ij}, K_{ij}^* = K_i^* \delta_{ij}, i \text{ is not summed } i, j \\ &= 1, 2, 3 \text{ and } \delta_{ij} \text{ is Kronecker delta.} \end{aligned}$$

Also the strain displacement relations are

$$e_{ij} = \frac{1}{2} (u_{i,j} + u_{j,i}), i, j = 1, 2, 3. \quad (9)$$

Following Youssef (2006), the two temperature relation is given by

$$T = \phi - a_{ij} \phi_{,ij}, \quad i, j = 1, 2, 3 \quad (10)$$

3. Formulation of the problem

We consider a perfectly conducting homogeneous orthotropic magneto-thermoelastic medium rotating with an angular velocity $\Omega = \Omega \vec{n}$ initially at uniform temperature T_0 in the context of three-phase-lag fractional order model of thermoelasticity with an initial magnetic field $\vec{H} =$

$(0, H_0, 0)$, towards y -axis. We take a rectangular coordinate system (x, y, z) having origin on the surface $z = 0$ with z -axis as a axis of symmetry and pointing vertically downwards into the medium. We choose x -axis in the direction of wave propagation so that all the particles on a line parallel to y -axis are equally displaced. Therefore, all the field quantities will be independent of y -coordinate. For the 2D problem in xz -plane, we take

$$u = u(x, z, t), v = 0, w = w(x, z, t), \phi = \phi(x, z, t), \quad (11)$$

Let us assume that

$$\mathbf{\Omega} = (0, \Omega, 0), \quad (12)$$

From the generalized ohm's law

$$J_2 = 0, \quad (13)$$

And the current density components are given by

$$J_1 = -\varepsilon_0 \mu_0 H_0 \frac{\partial^2 w}{\partial t^2}, \quad (14)$$

$$J_3 = \varepsilon_0 \mu_0 H_0 \frac{\partial^2 u}{\partial t^2}, \quad (15)$$

Following Kumar and Chawla (2014), the stress-strain relations in an orthotropic medium is given by

$$\sigma_{11} = C_{11} e_{11} + C_{13} e_{33} - \beta_1 T, \quad (16)$$

$$\sigma_{33} = C_{13} e_{11} + C_{33} e_{33} - \beta_3 T, \quad (17)$$

$$= 2C_{55} e_{13}, \quad (18)$$

Where

$$e_{11} = \frac{\partial u}{\partial x}, e_{33} = \frac{\partial w}{\partial z}, e_{13} = \frac{1}{2} \left(\frac{\partial u}{\partial z} + \frac{\partial w}{\partial x} \right), T = \phi - \left(a_1 \frac{\partial^2 \phi}{\partial x^2} + a_3 \frac{\partial^2 \phi}{\partial z^2} \right), \quad (19)$$

$$\beta_1 = C_{11} \alpha_1 + C_{13} \alpha_3, \beta_3 = C_{13} \alpha_1 + C_{33} \alpha_3.$$

Eqs. (6) and (8) with the aid of (9)-(10) and (11)-(19) reduce to the form

$$C_{11} \frac{\partial^2 u}{\partial x^2} + C_{55} \frac{\partial^2 u}{\partial z^2} + (C_{13} + C_{55}) \frac{\partial^2 w}{\partial x \partial z} - \beta_1 \frac{\partial}{\partial x} \left\{ \phi - \left(a_1 \frac{\partial^2 \phi}{\partial x^2} + a_3 \frac{\partial^2 \phi}{\partial z^2} \right) \right\} - \mu_0 J_3 H_0 = \rho \left(\frac{\partial^2 u}{\partial t^2} - \Omega^2 u + 2\Omega \frac{\partial w}{\partial t} \right), \quad (20)$$

$$(C_{55} + C_{13}) + C_{55} \frac{\partial^2 w}{\partial x^2} + C_{33} \frac{\partial^2 w}{\partial z^2} - \beta_3 \frac{\partial}{\partial z} \left\{ \phi - \left(a_1 \frac{\partial^2 \phi}{\partial x^2} + a_3 \frac{\partial^2 \phi}{\partial z^2} \right) \right\} + \mu_0 J_1 H_0 = \rho \left(\frac{\partial^2 w}{\partial t^2} - \Omega^2 w - 2\Omega \frac{\partial u}{\partial t} \right), \quad (21)$$

$$K_1 \left(1 + \frac{\tau_t^\alpha}{\alpha!} \frac{\partial}{\partial t^\alpha} \right) \phi_{,11} + K_3 \left(1 + \frac{\tau_t^\alpha}{\alpha!} \frac{\partial}{\partial t^\alpha} \right) \phi_{,33} + K_1^* \left(1 + \frac{\tau_v^\alpha}{\alpha!} \frac{\partial}{\partial t^\alpha} \right) \phi_{,11} + K_3^* \left(1 + \frac{\tau_v^\alpha}{\alpha!} \frac{\partial}{\partial t^\alpha} \right) \phi_{,33} = \left[1 + \frac{\tau_q^\alpha}{\alpha!} \frac{\partial}{\partial t^\alpha} + \frac{\tau_q^{2\alpha!}}{2\alpha!} \frac{\partial^2}{\partial t^{2\alpha}} \right] \left[\rho C_E \frac{\partial^2}{\partial t^2} \left\{ \phi - \left(a_1 \frac{\partial^2 \phi}{\partial x^2} + a_3 \frac{\partial^2 \phi}{\partial z^2} \right) \right\} + T_0 \left\{ \beta_1 \ddot{u}_{1,1} + \beta_3 \ddot{u}_{3,3} \right\} \right] \quad (22)$$

In the above equations, we use the contracting subscript notations

($11 \rightarrow 1, 22 \rightarrow 2, 33 \rightarrow 3, 23 \rightarrow 4, 13 \rightarrow 5, 12 \rightarrow 6$) to relate C_{ijkl} to C_{mn}

Where $i, j, k, l = 1, 2, 3$ and $m, n = 1, 2, 3, 4, 5, 6$

We assume that the medium is initially is at rest. Then the undisturbed state is maintained at reference temperature. Then the initial and regularity conditions are

$$u(x, z, 0) = 0 = \dot{u}(x, z, 0),$$

$$w(x, z, 0) = 0 = \dot{w}(x, z, 0),$$

$$\phi(x, z, 0) = 0 = \dot{\phi}(x, z, 0) \text{ for } x_3 \geq 0, -\infty < x_1 < \infty,$$

$$u(x, z, t) = w(x, z, t) = \phi(x, z, t) = 0 \text{ For } t > 0 \text{ when } x_3 \rightarrow \infty.$$

To facilitate the solution the following dimensionless quantities are used

$$\begin{aligned} x' = \frac{x}{L}, z' = \frac{z}{L}, u' = \frac{\rho c_1^2}{LT_0\beta_1} u, w' = \frac{\rho c_1^2}{LT_0\beta_1} w, t' = \frac{c_1}{L} t, \sigma'_{33} = \frac{\sigma_{33}}{T_0\beta_1}, \\ \sigma'_{31} = \frac{\sigma_{31}}{T_0\beta_1}, \phi' = \frac{\phi}{T_0}, \Omega' = \frac{L}{c_1} \Omega, a_1' = \frac{a_1}{L^2}, a_3' = \frac{a_3}{L^2}. \end{aligned} \quad (23)$$

Where, $c_1^2 = \frac{c_{11}}{\rho}$,

Using dimensionless quantities given by (23) in Eqs. (20)-(22) and suppressing the primes for convenience yield

$$\left(\frac{\partial^2 u}{\partial x^2} + \delta_1 \frac{\partial^2 u}{\partial z^2} + \delta_2 \frac{\partial^2 w}{\partial x \partial z} \right) - \frac{\partial}{\partial x} \left\{ \phi - \left(\frac{a_1}{L} \frac{\partial^2 \phi}{\partial x^2} + \frac{a_3}{L} \frac{\partial^2 \phi}{\partial z^2} \right) \right\} = \left\{ \left(1 + \frac{\varepsilon_0 \mu_0^2 H_0^2}{\rho} \right) \frac{\partial^2 u}{\partial t^2} - \Omega^2 u + 2\Omega \frac{\partial w}{\partial t} \right\}, \quad (24)$$

$$\left(\delta_3 \frac{\partial^2 w}{\partial z^2} + \delta_1 \frac{\partial^2 w}{\partial x^2} + \delta_2 \frac{\partial^2 u}{\partial x \partial z} \right) - \varepsilon \frac{\partial}{\partial z} \left\{ \phi - \left(\frac{a_1}{L} \frac{\partial^2 \phi}{\partial x^2} + \frac{a_3}{L} \frac{\partial^2 \phi}{\partial z^2} \right) \right\} = \left\{ \left(1 + \frac{\varepsilon_0 \mu_0^2 H_0^2}{\rho} \right) \frac{\partial^2 w}{\partial t^2} - \Omega^2 w - 2\Omega \frac{\partial u}{\partial t} \right\}, \quad (25)$$

$$\begin{aligned} \epsilon_1 T_1 \frac{\partial}{\partial t} \left(\frac{\partial^2 \phi}{\partial x^2} \right) + \epsilon_2 T_1 \frac{\partial}{\partial t} \left(\frac{\partial^2 \phi}{\partial z^2} \right) + \epsilon_3 T_2 \left(\frac{\partial^2 \phi}{\partial x^2} \right) + \epsilon_4 T_2 \left(\frac{\partial^2 \phi}{\partial z^2} \right) = T_3 \left[\frac{\partial^2}{\partial t^2} \left\{ \phi - \left(\frac{a_1}{L} \frac{\partial^2 \phi}{\partial x^2} + \frac{a_3}{L} \frac{\partial^2 \phi}{\partial z^2} \right) \right\} + \epsilon_5 \frac{\partial^2}{\partial t^2} \left(\frac{\partial u}{\partial x} + \varepsilon \frac{\partial w}{\partial z} \right) \right], \end{aligned} \quad (26)$$

Where,

$$\begin{aligned} \delta_1 = \frac{c_{55}}{c_{11}}, \delta_2 = \frac{c_{13} + c_{15}}{c_{11}}, \delta_3 = \frac{c_{33}}{c_{11}}, \epsilon_1 = \frac{K_1}{\rho L C_1 C_E}, \epsilon_2 = \frac{K_3}{\rho L C_1 C_E}, \epsilon_3 = \frac{K_1^*}{\rho c_1^2 C_E}, \epsilon_4 = \frac{K_3^*}{\rho c_1^2 C_E}, \\ \epsilon_5 = \frac{\beta_1^2 T_0}{\rho^2 c_1^2 C_E}, \varepsilon = \frac{\beta_3}{\beta_1}, T_1 = \left(1 + \frac{\tau_t^\alpha}{\alpha!} \frac{\partial^\alpha}{\partial t^\alpha} \right), T_2 = \left(1 + \frac{\tau_q^\alpha}{\alpha!} \frac{\partial^\alpha}{\partial t^\alpha} \right), T_3 = \left[1 + \frac{\tau_q^\alpha}{\alpha!} \frac{\partial^\alpha}{\partial t^\alpha} + \frac{\tau_q^{\alpha!}}{2\alpha!} \frac{\partial^{2\alpha}}{\partial t^{2\alpha}} \right]. \end{aligned}$$

4. Solution of the problem

Following Kaur *et al.* (2021), we take harmonic plane wave solution of the form

$$\begin{pmatrix} u \\ w \\ \phi \end{pmatrix} = \begin{pmatrix} u^* \\ w^* \\ \phi^* \end{pmatrix} \exp\{i(\xi x n_1 + \xi z n_3 - \omega t)\}, \quad (27)$$

Where (n_1, n_3) denotes the projection of the wave normal onto the $x - z$ plane, ξ and ω are respectively the wave number and angular frequency of plane harmonic waves propagating in $x -$

z plane.

Upon using Eq. (27) in Eqs. (24)-(26) and eliminating u^* , w^* and ϕ^* from the resulting equations yields the following characteristic equation.

$$(A\xi^6 + B\xi^4 + C\xi^2 + D) = 0, \quad (28)$$

Where,

$$\begin{aligned} A &= [p_1 p_9 p_{15} - p_1 p_{12} p_{14} - p_3 p_7 p_{15} + p_3 p_{12} p_{13} + p_6 p_7 p_{14} - p_6 p_9 p_{13}], \\ B &= [p_1 p_9 p_{16} + p_1 p_{10} p_{15} - p_1 p_{11} p_{14} + p_2 p_9 p_{15} - p_2 p_{12} p_{14} - p_3 p_7 p_{16} - p_3 p_8 p_{15} + \\ &\quad p_3 p_{11} p_{13} - p_4 p_7 p_{15} + p_4 p_{12} p_{13} + p_5 p_7 p_{14} - p_5 p_9 p_{13} + p_6 p_8 p_{14} - p_6 p_{10} p_{13}], \\ C &= [p_1 p_{10} p_{16} + p_2 p_9 p_{16} + p_2 p_{10} p_{15} - p_2 p_{11} p_{14} - p_3 p_8 p_{16} - p_4 p_7 p_{16} - p_4 p_8 p_{15} + \\ &\quad p_4 p_{11} p_{13} + p_5 p_8 p_{14} - p_5 p_{10} p_{13}], \\ D &= [p_2 p_{10} p_{16} - p_4 p_8 p_{16}], \\ p_1 &= [-n_1^2 - \delta_1 n_3^2], \\ p_2 &= \Omega^2 + \omega^2 \left(1 + \frac{\varepsilon_0 \mu_0^2 H_0^2}{\rho} \right), \\ p_3 &= -\delta_2 n_1 n_3, \\ p_4 &= 2\Omega i \omega, \\ p_5 &= -i n_1, \\ p_6 &= -i a_1 n_1^3 + i a_3 n_1 n_3^2, \\ p_7 &= p_3, \\ p_8 &= -p_4, \\ p_9 &= -\delta_1 n_1^2 - \delta_3 n_3^2, \\ p_{10} &= p_2, \\ p_{11} &= -i \varepsilon n_3, \\ p_{12} &= -i \varepsilon a_1 n_1^2 n_3 + i \varepsilon a_3 n_3^3, \\ p_{13} &= T_3' i \varepsilon_5 \omega^2 n_1, \\ p_{14} &= T_3' i \varepsilon \varepsilon_5 \omega^2 n_3, \\ p_{15} &= T_1' [i \varepsilon_1 \omega n_1^2 + i \varepsilon_2 \omega n_3^2] + T_2' [-\varepsilon_3 n_1^2 - \varepsilon_4 n_3^2] - T_3' \omega^2 [a_1 n_1^2 + a_3 n_3^2], \\ p_{16} &= T_3' \omega^2, \\ T_1' &= 1 + \frac{\tau_t^\alpha}{\alpha!} (-i\omega)^\alpha, \\ T_2' &= 1 + \frac{\tau_v^\alpha}{\alpha!} (-i\omega)^\alpha, \\ T_3' &= 1 + \frac{\tau_q^\alpha}{\alpha!} (-i\omega)^\alpha + \frac{\tau_q^{2\alpha}}{2\alpha!} (-i\omega)^{2\alpha}. \end{aligned}$$

The roots of the Eq. (28) gives six values of ξ , in which we are interested in those roots whose imaginary parts are positive. Corresponding to these roots, there exist three waves corresponding to decreasing orders of their velocities, namely quasi-longitudinal, quasi-transverse and quasi-thermal waves. The phase velocities, attenuation coefficients, specific loss and penetration depth of these waves are obtained by the following expressions.

(i) *Phase velocity*

The phase velocity is given by

$$V_j = \frac{\omega}{|Re(\xi_j)|}, \quad j = 1, 2, 3 \quad (29)$$

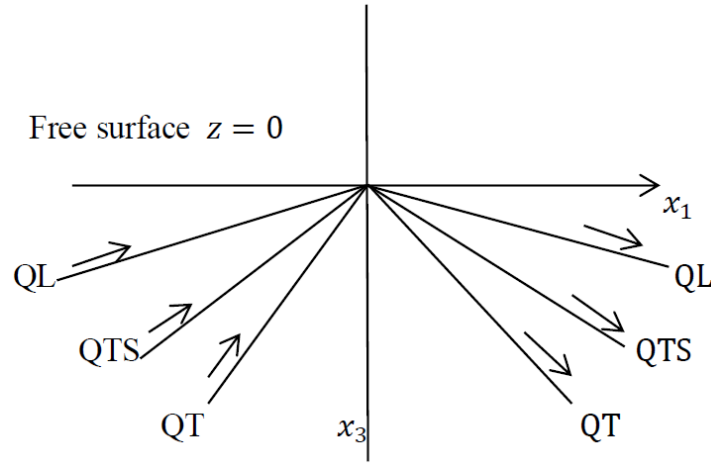


Fig. 1 Geometry of the problem

Where, $V_j, j = 1,2,3$ are the phase velocities of QL, QTS and QT-waves respectively.

(ii) *Attenuation coefficient*

The attenuation coefficient is defined by

$$Q_j = \text{Im}(\xi_j), j = 1,2,3 \quad (30)$$

Where, $Q_j, j = 1,2,3$ are the attenuation coefficients of QL, QTS and QT-waves respectively.

(iii) *Specific loss*

The specific loss is the ratio of the energy (Δw) dissipated in taking a specimen through a stress cycle, to the elastic energy (w) stored in the specimen when the strain is maximum. The specific loss is defined as

$$W_j = \left(\frac{\Delta w}{w}\right)_j = 4\pi \left| \frac{\text{img}(\xi_j)}{\text{Re}(\xi_j)} \right|, j = 1,2,3 \quad (31)$$

Where, $W_j, j = 1,2,3$ are the specific losses of QL, QTS and QT waves respectively.

(iv) *Penetration depth*

The penetration depth is defined as

$$S_j = \frac{1}{|\text{img}(\xi_j)|}, \quad j = 1,2,3 \quad (32)$$

=where $S_j, j = 1,2,3$ are the penetration depths of QL, QTS and QT waves respectively.

5. Reflection and transmission at the boundary surfaces

We consider an orthotropic magneto-thermoelastic half-space occupying the region $z \geq 0$. Incident quasi-longitudinal or quasi-transverse or quasi-thermal waves at the stress free surface ($z = 0$) will generate QL-reflected, QTS-reflected and QT-reflected waves in the half-space $z > 0$. The total displacements, conductive temperature are given by

$$u = \sum_{j=1}^6 A_j e^{iM_j}, w = \sum_{j=1}^6 d_j A_j e^{iM_j}, \phi = \sum_{j=1}^6 l_j A_j e^{iM_j}; j = 1, 2, \dots, 6 \quad (33)$$

Where,

$$M_j = \omega t - \xi_j (x n_{1j} - z n_{3j}), \quad j = 1, 2, 3$$

$$M_j = \omega t - \xi_j (x n_{1j} + z n_{3j}), \quad j = 4, 5, 6$$

Here the subscripts $j = 1, 2, 3$ respectively denote the quantities corresponding to incident QL, QTS, QT waves and the subscripts $j = 4, 5, 6$ denote the corresponding reflected QL, QTS and QT-waves, ξ_j denotes the roots of the Eq. (28), $n_{1j} = \sin\theta_j$, $n_{3j} = \cos\theta_j$.

$$d_j = \frac{\xi_j^4 (p_{1j} p_{15j} - p_{6j} p_{13j}) + \xi_j^2 (p_{1j} p_{16j} + p_{2j} p_{15j} - p_{5j} p_{13j}) + p_2 p_{16}}{\xi_j^4 (p_{9j} p_{15j} - p_{12j} p_{14j}) + \xi_j^2 (p_{9j} p_{16j} + p_{10j} p_{15j} - p_{11j} p_{14j}) + p_{10} p_{16}},$$

$$l_j = \frac{\xi_j^4 (p_{1j} p_{9j} - p_{3j} p_{7j}) + \xi_j^2 (p_{1j} p_{10j} + p_{2j} p_{9j} - p_{3j} p_{8j} - p_{4j} p_{7j}) + (p_2 p_{10} - p_4 p_8)}{\xi_j^4 (p_{9j} p_{15j} - p_{12j} p_{14j}) + \xi_j^2 (p_{9j} p_{16j} + p_{10j} p_{15j} - p_{11j} p_{14j}) + p_{10} p_{16}},$$

for $j = 1, 2, 3$

$$d_j = \frac{\xi_j^4 (p_{1j} p_{15j} - p_{6j} p_{13j}) + \xi_j^2 (p_{1j} p_{16j} + p_{2j} p_{15j} - p_{5j} p_{13j}) + p_2 p_{16}}{\xi_j^4 (p_{9j} p_{15j} + p_{12j} p_{14j}) + \xi_j^2 (p_{9j} p_{16j} + p_{10j} p_{15j} - p_{11j} p_{14j}) + p_{10} p_{16}},$$

$$l_j = \frac{\xi_j^4 (p_{1j} p_{9j} - p_{3j} p_{7j}) + \xi_j^2 (p_{1j} p_{10j} + p_{2j} p_{9j} + p_{3j} p_{8j} + p_{4j} p_{7j}) + (p_2 p_{10} - p_4 p_8)}{\xi_j^4 (p_{9j} p_{15j} + p_{12j} p_{14j}) + \xi_j^2 (p_{9j} p_{16j} + p_{10j} p_{15j} - p_{11j} p_{14j}) + p_{10} p_{16}},$$

for $j = 4, 5, 6$

6. Boundary conditions

Following Lata *et al.* (2016), we take the following boundary conditions at the free surface $z = 0$

$$(1) \sigma_{33} = 0, \quad (34)$$

$$(2) \sigma_{31} = 0, \quad (35)$$

$$(3) \frac{\partial \phi}{\partial z} = 0 \text{ at } z = 0, \quad (36)$$

Making the use of Eq. (33) in (34)-(36), we obtain

$$\sum_{j=1}^3 (-i\xi_j \sin\theta_j \frac{c_{13}}{\rho c_1^2} + i\xi_j d_j \cos\theta_j \frac{c_{33}}{\rho c_1^2} - \varepsilon l_j (1 + a_1 \xi_j^2 \sin^2\theta_j + a_3 \xi_j^2 \cos^2\theta_j)) A_j e^{iM_j(x,0)} + \sum_{j=4}^6 (-i\xi_j \sin\theta_j \frac{c_{13}}{\rho c_1^2} - i\xi_j d_j \cos\theta_j \frac{c_{33}}{\rho c_1^2} - \varepsilon l_j (1 + a_1 \xi_j^2 \sin^2\theta_j + a_3 \xi_j^2 \cos^2\theta_j)) A_j e^{iM_j(x,0)} = 0, \quad (37)$$

$$\sum_{j=1}^3 (i\xi_j \cos\theta_j - i\xi_j d_j \sin\theta_j) A_j e^{iM_j(x,0)} + \sum_{j=4}^6 (-i\xi_j \cos\theta_j - i\xi_j d_j \sin\theta_j) A_j e^{iM_j(x,0)} = 0, \quad (38)$$

$$\sum_{j=1}^3 (i\xi_j l_j \cos\theta_j) A_j e^{iM_j(x,0)} + \sum_{j=4}^6 (-i\xi_j l_j \cos\theta_j) A_j e^{iM_j(x,0)} = 0, \quad (39)$$

The Eqs. (37)-(39) are satisfied for all values of x , therefore we have

$$M_1(x, 0) = M_2(x, 0) = M_3(x, 0) = M_4(x, 0) = M_5(x, 0) = M_6(x, 0), \quad (40)$$

From the equations (33) and (40), we obtain

$$\xi_1 \sin \theta_1 = \xi_2 \sin \theta_2 = \xi_3 \sin \theta_3 = \xi_4 \sin \theta_4 = \xi_5 \sin \theta_5 = \xi_6 \sin \theta_6, \quad (41)$$

Which is the form of Snell's law for stress free surface of orthotropic magneto-thermoelastic medium with rotation, the Eqs. (33)-(35) and (37) yield

$$\sum_{q=1}^3 X_{iq} A_q + \sum_{j=4}^6 X_{ij} A_j = 0, \quad i = 1, 2, 3 \quad (42)$$

Where

$$\begin{aligned} X_{1q} &= (-i\xi_q \sin \theta_q \frac{c_{13}}{\rho c_1^2} + i\xi_q d_q \cos \theta_q \frac{c_{33}}{\rho c_1^2} - \varepsilon l_q (1 + a_1 \xi_q^2 \sin^2 \theta_q + a_3 \xi_q^2 \cos^2 \theta_q)), \quad q = \\ &\quad 1, 2, 3 \\ X_{2q} &= (i\xi_q \cos \theta_q - i\xi_q d_q \sin \theta_q), \quad q = 1, 2, 3 \\ X_{3q} &= (i\xi_q l_q \cos \theta_q), \quad q = 1, 2, 3 \\ X_{1j} &= (-i\xi_j \sin \theta_j \frac{c_{13}}{\rho c_1^2} - i\xi_j d_j \cos \theta_j \frac{c_{33}}{\rho c_1^2}) - \varepsilon l_j (1 + a_1 \xi_j^2 \sin^2 \theta_j + a_3 \xi_j^2 \cos^2 \theta_j), \quad j = \\ &\quad 4, 5, 6 \\ X_{2j} &= (i\xi_j \cos \theta_j - i\xi_j d_j \sin \theta_j), \quad j = 4, 5, 6 \\ X_{3j} &= (-i\xi_j l_j \cos \theta_j), \quad j = 4, 5, 6 \end{aligned} \quad (43)$$

7. Amplitude ratios

7.1 Incident QL-wave

In case of Quasi-longitudinal wave, the subscript q takes only one value, that is $q = 1$ which means $A_2 = A_3 = 0$, dividing the set of Eq. (38) throughout by A_1 then we obtain a system of three non-homogeneous equations in three unknowns which is solved by Cramer's rule and we have

$$A_{1i} = \frac{A_{i+3}}{A_1} = \frac{\Delta_i^1}{\Delta}, \quad i = 1, 2, 3 \quad (44)$$

7.2 Incident QTS-wave

In case of Quasi-longitudinal wave, the subscript q takes only one value, that is $q = 2$ which means $A_1 = A_3 = 0$, dividing the set of Eq. (38) throughout by A_2 , we obtain a system of three non-homogeneous equations in three unknowns which is solved by Cramer's rule and we get

$$A_{2i} = \frac{A_{i+3}}{A_2} = \frac{\Delta_i^2}{\Delta}, \quad i = 1, 2, 3 \quad (45)$$

7.3 Incident QT-wave

In case of Quasi-longitudinal wave, the subscript q takes only one value, that is $q = 3$ which

means $A_1 = A_2 = 0$, dividing the set of Eq. (38) throughout by A_3 then we obtain a system of three non-homogeneous equations in three unknowns which is solved by Cramer's rule and we have

$$A_{3i} = \frac{A_{i+3}}{A_3} = \frac{\Delta_i^3}{\Delta}, \quad i = 1,2,3 \quad (46)$$

Where,

A_{1i}, A_{2i}, A_{3i} are the amplitude ratios of the reflected QL, reflected QTS and reflected QT waves respectively.

Here $\Delta = |X_{ii+3}|_{3 \times 3}$ and $\Delta_i^p, (i = 1,2,3)$ can be obtained by replacing, respectively, 1st, 2nd, and 3rd columns of Δ by $[-X_{1p}, -X_{2p}, -X_{3p}]^t$

Following Achenbach (1973), the energy flux across the surface element, which is the rate at which energy is communicated per unit area of the area of the surface, is repeated as

$$P^* = t_{lm} n_m \dot{u}_l, \quad (47)$$

Where, t_{lm} is the stress tensor, n_m are the direction cosines of the unit normal and \dot{u}_l are the components of the particle velocity.

The time average of P^* over a period, denoted by $\langle P^* \rangle$ represents the average energy transmission per unit surface area per unit time and is given at the interface $x_3 = 0$, as

$$\langle P^* \rangle = \langle \text{Re}(t_{13}) \cdot \text{Re}(u_1) + \text{Re}(t_{33}) \cdot \text{Re}(u_3) \rangle, \quad (48)$$

8. Energy ratios

Following Achenbach (1973), for any two complex functions f and g , we have

$$\langle \text{Re}(f) \rangle \langle \text{Re}(g) \rangle = \frac{1}{2} \text{Re}(f \bar{g}), \quad (49)$$

The expressions for energy ratio $E_i, (i = 1,2,3)$ for reflected QL, QTS and QT waves is given as

8.1 Incident QL-wave

$$E_{1i} = \frac{\langle P_{i+3}^* \rangle}{\langle P_1^* \rangle}, \quad i = 1,2,3 \quad (50)$$

8.2 Incident QTS-wave

$$E_{2i} = \frac{\langle P_{i+3}^* \rangle}{\langle P_2^* \rangle}, \quad i = 1,2,3 \quad (51)$$

8.3 Incident QT-wave

$$E_{3i} = \frac{\langle P_{i+3}^* \rangle}{\langle P_3^* \rangle}, \quad i = 1,2,3 \quad (52)$$

Where, $\langle P_i^* \rangle$ $i = 1,2,3$ are the average energies transmission per unit surface area per unit time corresponding to incident QL, QTS, and QT waves respectively and $\langle P_{i+3}^* \rangle$ $i = 1,2,3$ is the average energies transmission per unit surface area per unit time corresponding to reflected QL, QTS and QT waves respectively.

9. Particular cases

1. If we put $K_1 = K_3 = 0$ in Eq. (22), the problem reduces for the case Plane harmonic wave propagation in orthotropic magneto-thermoelastic rotating medium without energy dissipation (GN-II type) with three-phase-lag fractional order model and two-temperature.

2. If $C_{11} = C_{33}$, $2C_{55} = C_{11} - C_{33}$, we get the expressions for Plane harmonic wave propagation in transversely isotropic magneto-thermoelastic medium with combined effect of rotation and two-temperature with GN-III type fractional order model with three-phase-lags.

3. If $C_{11} = C_{33} = \lambda + 2\mu$, $C_{13} = \lambda$, $C_{55} = \mu$, $\beta_1 = \beta_3 = \beta$, $K_1 = K_3 = K$, $K_1^* = K_3^* = K^*$, we get the expressions for Plane harmonic wave propagation for isotropic solid with three-phase-lag fractional order theory in generalized thermoelasticity.

4. If we put $\tau_t = \tau_v = \tau_q = 0$, and $K_1^* = K_3^* = 0$, in Eq. (22) then the resulting equation represents heat equation for coupled theory of thermoelasticity.

5. If we put $K_1^* = K_3^* = 0$, in Eq. (22), then the problem reduces for the case GN-I type fractional order model in generalized thermoelasticity.

6. If we put $\tau_t = \tau_v = \tau_q = 0$, in Eq. (22), then the resulting equation reduces for the case GN-III type model of thermoelasticity.

7. If we put $a_1 = a_3 = 0$, in Eq. (22), the problem reduces for the case Plane wave propagation in orthotropic magneto-thermoelastic rotating medium without two-temperature and with three-phase-lag fractional order model in generalized thermoelasticity.

8. If $\Omega = 0$, then we obtain the corresponding expressions for an orthotropic magneto-thermoelastic solid with and without energy dissipation and with two-temperature without rotation.

10. Numerical results and discussion

Following Lata and Himanshi (2021a), for the purpose of numerical calculation cobalt material has been taken for the purpose of numerical computations with numerical values as

$$\begin{aligned} c_{11} &= 3.071 \times 10^{11} \text{ Kgm}^{-1}\text{s}^{-2}, c_{13} = 1.650 \times 10^{11} \text{ Kgm}^{-1}\text{s}^{-2}, c_{33} = 3.581 \times \\ &10^{11} \text{ Kgm}^{-1}\text{s}^{-2}, \\ c_{55} &= 1.510 \times 10^{11} \text{ Kgm}^{-1}\text{s}^{-2}, c_E = 4.27 \times 10^2 \text{ JKg}^{-1}\text{K}^{-1}, \beta_1 = 7.04 \times 10^6 \text{ Nm}^2\text{K}^{-1}, \\ \beta_3 &= 6.90 \times 10^6 \text{ Nm}^2\text{K}^{-1}, T_0 = 293\text{K}, K_1 = 6.90 \times 10^2 \text{ Wm}^{-1}\text{K}^{-1}, K_3 = 7.01 \times \\ &10^2 \text{ Wm}^{-1}\text{K}^{-1}, \\ K_1^* &= 1.313 \times 10^2 \text{ Ws}^{-1}, K_3^* = 1.54 \times 10^2 \text{ Ws}^{-1}, \rho = 8.836 \times 10^3 \text{ Kgm}^{-3}, \tau_v = 2.0 \times 10^{-7} \text{ S}, \\ \tau_q &= 2.0 \times 10^{-7} \text{ S}, \mu_0 = 1.2571 \times 10^{-6} \text{ Hm}^{-1}, H_0 = 1 \text{ Jm}^{-1}\text{nb}^{-1}, \epsilon_0 = 8.838 \times 10^{-12} \text{ Fm}, \\ \tau_t &= 2.0 \times 10^{-7} \text{ S}, L = 1 \end{aligned}$$

Using the above values, the numerical simulated results are represented graphically with the help of octave software. The variations of phase velocity, attenuation coefficient depth, Specific loss, penetration depth, amplitude ratios and energy ratios of the reflected QL, QTS, QT with

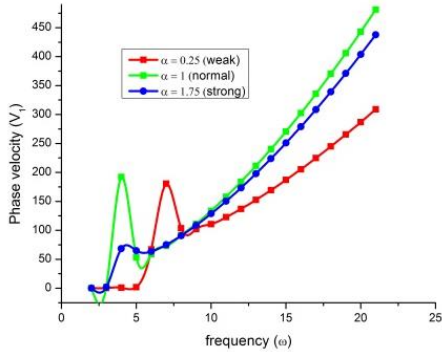


Fig. 2 Variation of phase velocity V_1 with frequency ω

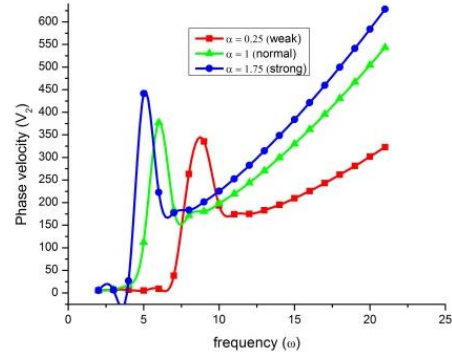


Fig. 3 Variation phase velocity V_2 with frequency ω

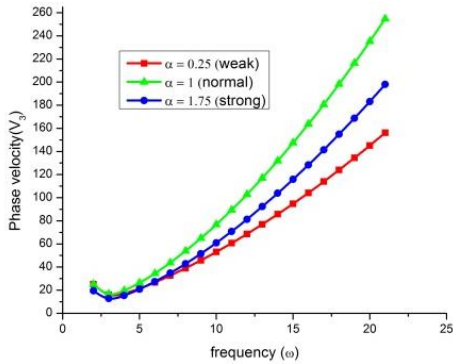


Fig. 4 Variation phase velocity V_3 with respect to frequency ω

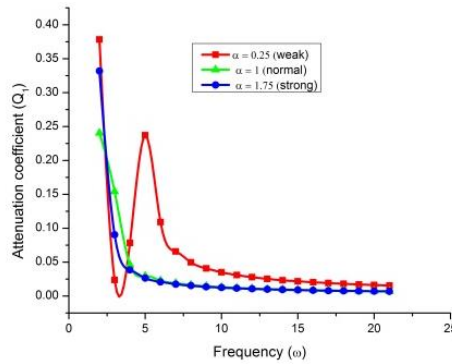


Fig. 5 Variation attenuation coefficient Q_1 with respect to frequency ω

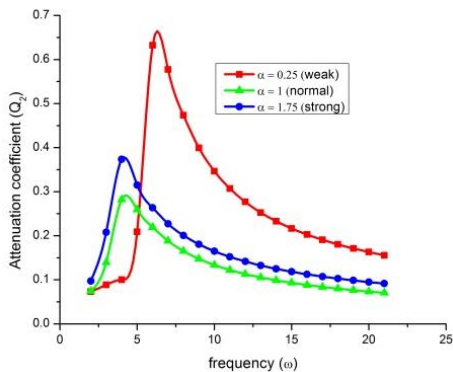


Fig. 6 Variation attenuation coefficient Q_2 with respect to frequency ω

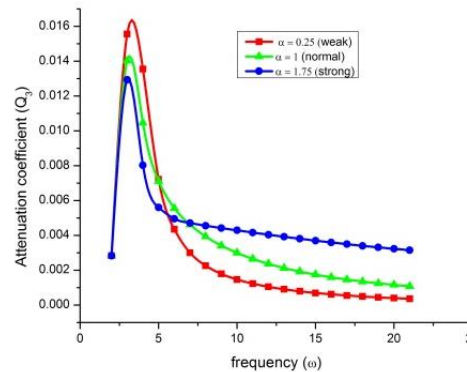


Fig. 7 Variation attenuation coefficient Q_3 with respect to frequency ω

respect to incident QL, QTS, QT corresponding to three different values of fractional parameter have been investigated for plane harmonic waves in an orthotropic magneto-thermoelastic rotating media in generalized thermoelasticity with three-phase-lag fractional order theory and two-

temperature. The variation of magnitude of phase velocity, attenuation coefficients, penetration depth and specific loss with respect to frequency are shown in Figs. 2-13. The variations of amplitude ratios and energy ratios of the reflected waves subject to incident waves with respect to angle of incidence have been plotted in Figs. 14-31 respectively.

11. Effect of fractional parameter

1. The red solid line with centre symbol (\square) relates to $\alpha = 0.25$ (weak conductivity)
2. The green solid line with centre symbol (Δ) relates to $\alpha = 1$ (normal conductivity)
3. The blue solid line with centre symbol (\circ) relates to $\alpha = 1.75$ (strong conductivity)

11.1 Phase velocity:

Figs. 2-4 gives the variation in the phase velocities V_1, V_2, V_3 with respect to frequency ω corresponding to three different values of fractional parameter $\alpha = 0.25, 1, 1.75$ respectively. We see that for all values of α the value of phase velocity V_1 oscillates in the range $2.5 \leq \omega \leq 7.5$ then increases monotonically corresponding to all values of α with different magnitudes. The phase velocity V_1 attains its maximum value corresponding to $\alpha = 1$ and attains minimum value corresponding to $\alpha = 0.25$ whereas the value corresponding to $\alpha = 1.75$ lies in between these two. Fig. 3 shows the behaviour of phase velocity V_2 with respect to frequency ω . We noticed that for $\alpha = 0.25, 1, 1.75$ in the starting range $2.5 \leq \omega \leq 10$ the value of phase velocity V_2 oscillates with different amplitude of oscillations then increases monotonically in the rest and attains a peak value for $\alpha = 1.75$ and minimum value for $\alpha = 0.25$ while for $\alpha = 1$ its value lies in between these two. Fig. 4, exhibits the nature of phase velocity V_3 with respect to frequency ω . It can be observed that its value decreases initially near the boundary surface then a sharp increase is noticed as the frequency increases for all values of $\alpha = 0.25, 1, 1.75$ respectively.

11.2 Attenuation coefficients:

Figs. 5-7 gives the variation in the value of attenuation coefficients Q_1, Q_2 and Q_3 with respect to frequency corresponding to three different values of fractional parameter $\alpha = 0.25, 1, 1.75$ respectively. Fig. 5 shows the variations in the attenuation coefficient Q_1 with respect to frequency ω . Here, we noticed that its value decreases sharply in the starting range $2.5 \leq \omega \leq 7.5$ for all values of $\alpha = 0.25, 1, 1.75$ respectively afterwards shows linearity. While for $\alpha = 0.25$ its value oscillates in the range $2.5 \leq \omega \leq 7.5$ then decreases and remains constant as the frequency approaches to its maximum value. The change in attenuation coefficient Q_2 is described in Fig. 6. We see that for $\alpha = 1, 1.75$ its value increases in the range $2.5 \leq \omega \leq 5$ then decreases slowly when frequency approaches to its maximum value. For $\alpha = 0.25$ in the range $2.5 \leq \omega \leq 7.5$ its value increases sharply and attains a highest peak at $\omega = 7.5$ afterwards declines in the rest. Fig. 7 represents the change in the attenuation coefficient Q_3 with respect to frequency ω . The value of Q_3 increases sharply in the starting range $2.5 \leq \omega \leq 4$ after that declines with different magnitude values corresponding to all values of $\alpha = 0.25, 1, 1.75$ respectively.

11.3 Specific loss

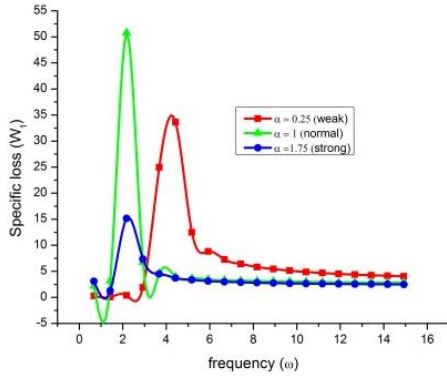


Fig. 8 Variation of specific loss W_1 with respect to frequency ω

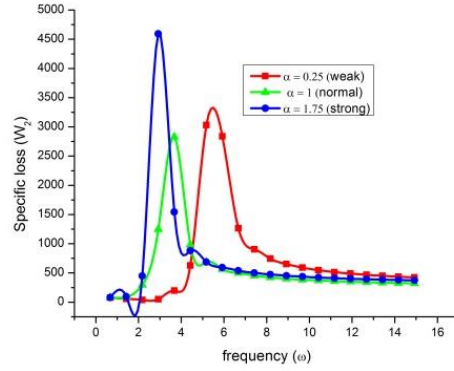


Fig. 9 Variation of specific loss W_2 with respect to frequency ω

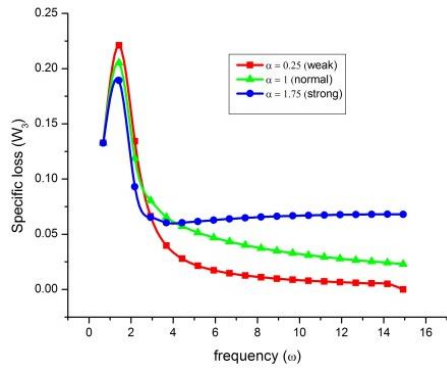


Fig. 10 Variation of specific loss W_3 with respect to frequency ω

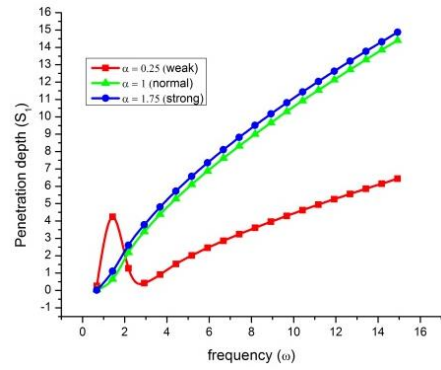


Fig. 11 Variation of penetration depth S_1 with respect to frequency ω

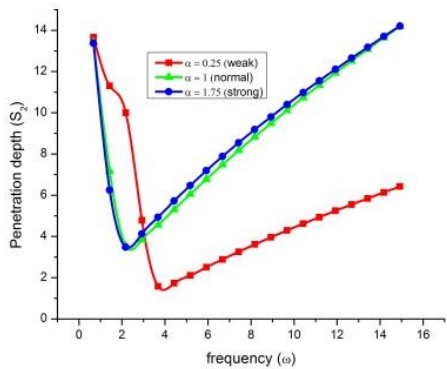


Fig. 12 Variation of penetration depth S_2 with respect to frequency ω

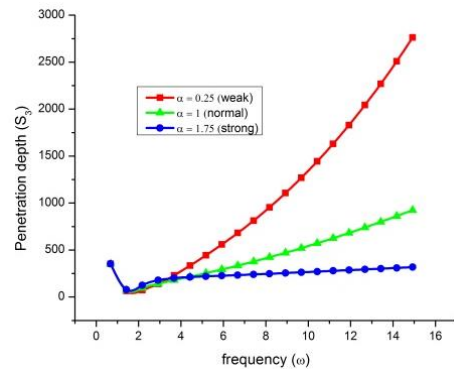


Fig. 13 Variation of penetration depth S_3 with respect to frequency ω

Figs. 8-10 gives the variation of specific loss W_1, W_2 and W_3 with respect to frequency corresponding to three different values of fractional parameter $\alpha = 0.25, 1, 1.75$ respectively. From Fig. 8 we observe that for $\alpha = 0.25$ the value of specific loss W_1 remains same in the range $0 \leq$

$\omega \leq 3$ then oscillates in the range $3 \leq \omega \leq 4$ and attains its maximum value at $\omega = 5$ after that its value declines in the remaining range. However, for $\alpha = 1, 1.75$, its value oscillates in the range $0 \leq \omega \leq 3$ then remains constant with increase in the value of frequency. Fig. 9 gives the variation of specific loss W_2 with respect to frequency ω . It can be noticed that for all the three cases trends are similar (oscillatory) with different magnitudes. Fig. 10 exhibits the variation of specific loss W_3 . We see that near the boundary the value of W_3 increases for all values of $\alpha=0.25, 1, 1.75$ respectively in the range $0 \leq \omega \leq 1$ and declines in the rest of the range. Further the value remains same throughout as the frequency approaches to its maximum value.

11.4 Penetration depth:

Figs. 11-13 gives the variation of penetration depth S_1, S_2 and S_3 with respect to frequency corresponding to three different values of fractional parameter $\alpha = 0.25, 1, 1.75$ respectively. For $\alpha = 0.25$. We observed that the value of penetration depth S_1 oscillates in the range $1 \leq \omega \leq 3$ afterwards increases monotonically in the rest. For $\alpha = 1, 1.75$ curves are increasing sharply in the whole range and attains a maximum value. Fig. 12 describes the nature of penetration depth S_2 with respect to frequency. The behaviour is quite opposite as compared to S_1 means its value decreases sharply near the boundary in the range $1 \leq \omega \leq 4$ afterwards increases monotonically in the rest. For $\alpha = 1, 1.75$ its value declines in the range $1 \leq \omega \leq 2$ after that it increases monotonically in the remaining range and attains a peak value with the increase in the value of frequency. The value of S_3 for $\alpha=0.25$ increases monotonically throughout. However for $\alpha=1, 1.75$ curves show small increase in its value in the whole range.

12. Amplitude ratios

12.1 Incident QL-wave

Figs. 14-16 depicts the variations of amplitude ratios A_{11}, A_{12}, A_{13} of QL-wave with respect to angle of incidence θ . From Fig. 14, we noticed that initially there is a small increase in the value of the amplitude ratio A_{11} for $\alpha=0.25$ and then declines monotonically with the increasing value of angle of incidence θ . For $\alpha=1, 1.75$ it decreases sharply near the boundary then a little increase is noticed after that its value decreases monotonically in the rest of the range and all the three curves intersect each other. From the Fig. 15, we conclude that initially in the range $0 \leq \theta \leq 19$ for $\alpha=1, 1.75$ the value of amplitude ratio A_{12} declines sharply then increases in the range $19 \leq \theta \leq 50$ afterwards its value decreases as the angle of incidence approaches to its maximum value. It can also be noticed that corresponding to all values of fractional parameter α and at $\theta = 90^\circ$ all the curves meet each other. The nature of amplitude ratio A_{13} is described in Fig. 16. Here, we noticed that behaviour is same as for the amplitude ratio A_{11} with different magnitude values.

12.2 Incident QTS-wave

Figs. 17-19 depicts the variations of amplitude ratios A_{21}, A_{22}, A_{23} of QTS-wave with respect to angle of incidence θ . From Fig. 17 it can be observed in the range $0 \leq \theta \leq 90$ the value of amplitude ratio A_{21} declines monotonically from its highest value to lowest value with different

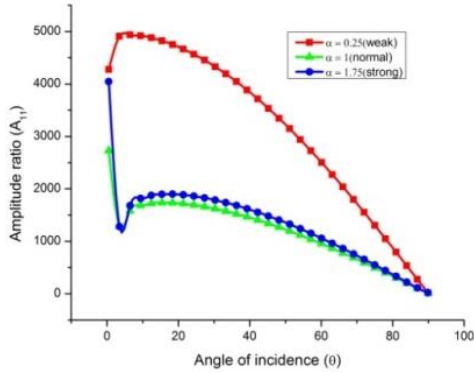


Fig. 14 Variation of amplitude ratio of A_{11} with respect of angle of incidence θ

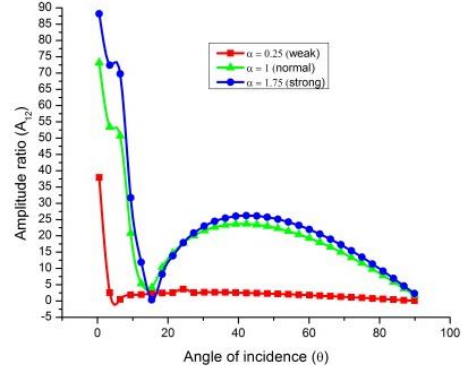


Fig. 15 Variation of amplitude ratio of A_{12} with respect of angle of incidence θ

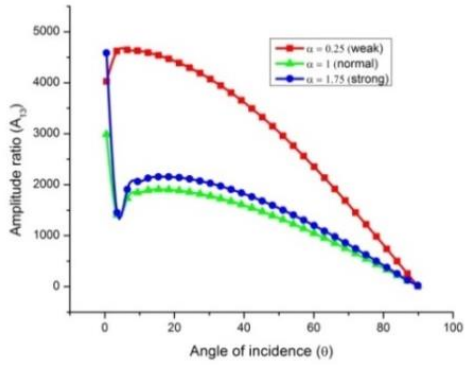


Fig. 16 Variation of amplitude ratio of A_{13} with respect of angle of incidence θ

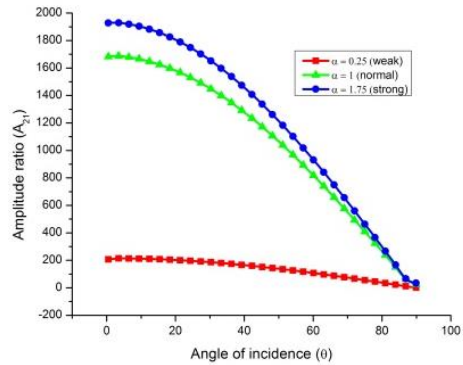


Fig. 17 Variation of amplitude ratio of A_{21} with respect of angle of incidence θ

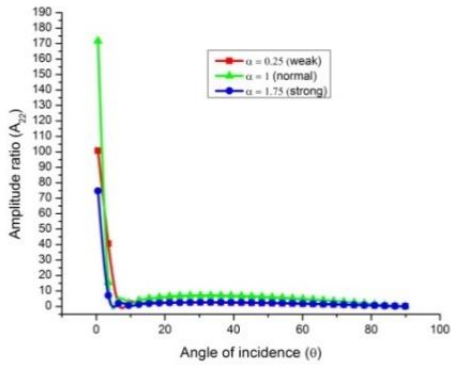


Fig. 18 Variation of amplitude ratio of A_{22} with respect of angle of incidence θ

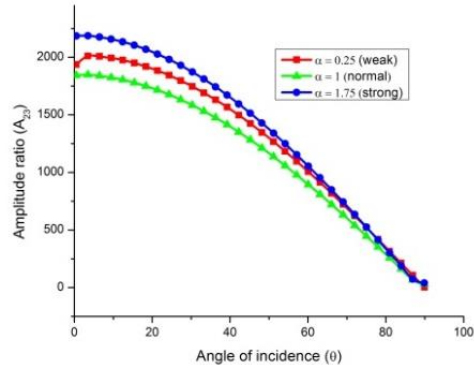


Fig. 19 Variation of amplitude ratio of A_{23} with respect of angle of incidence θ

magnitudes corresponding to all three values of $\alpha=0.25, 1, 1.75$ respectively. The change in the amplitude ratio A_{22} has shown in Fig. 18. It can be seen that in the range $0 \leq \theta \leq 10$ for all the three cases its value decreases sharply then remains constant with increase in the value of angle of incidence. The variation of amplitude ratio A_{23} is depicted in Fig. 19. We observed that variations are similar as for A_{21} with differ in their magnitude values. Further we also noticed that

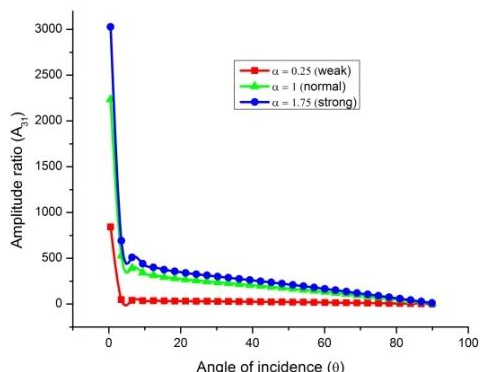


Fig. 20 Variation of amplitude ratio of A_{31} with respect of angle of incidence θ

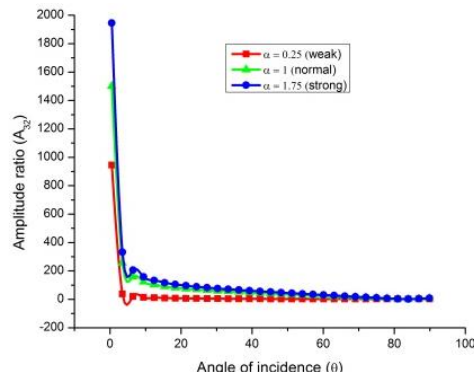


Fig. 21 Variation of amplitude ratio of A_{32} with respect of angle of incidence θ

corresponding to all values of fractional parameter α and at $\theta = 90^\circ$ all the curves meet each other.

12.3 Incident QT-wave

Figs. 20-22 gives the change in the value of amplitude ratios A_{31}, A_{32}, A_{33} of QT-wave with respect to angle of incidence θ . From the graphs it is clear that the value of all the three amplitude ratios A_{31}, A_{32}, A_{33} decreases monotonically from maximum to minimum value in range $0 \leq \theta \leq 5$ afterwards remains constant in the rest of the range corresponding to all three values of $\alpha=0.25, 1, 1.75$ respectively.

13. Energy ratios

13.1 Incident QL-wave

Figs. 23-25 depicts the variations of energy ratios E_{11}, E_{12}, E_{13} of QL-wave with respect to angle of incidence θ . It is clear from the Fig. 23 that for $\alpha=0.25, 1$ the value of energy ratio E_{11} increases monotonically. While for $\alpha=1.75$ its value decreases monotonically in the whole range of angle of incidence. The value of energy ratio E_{12} rises from low to high value with increase in the angle of incidence θ corresponding to all values of fractional parameter. It can be observed from fig 25 that the value of energy ratio E_{13} decreases in all the three cases with different magnitudes for $\alpha=0.25, 1, 1.75$ respectively.

13.2 Incident QTS-wave

Figs. 26-28 depicts the variations of energy ratios E_{21}, E_{22}, E_{23} of QTS-wave with respect to angle of incidence θ . we see that for $\alpha=0.25, 1$ the value of energy ratio E_{21} increases linearly while for $\alpha=1.75$ it decreases throughout with the increasing value of angle of incidence. The nature of energy ratio E_{22} has shown in Fig. 27. From the graph it can be seen that its value

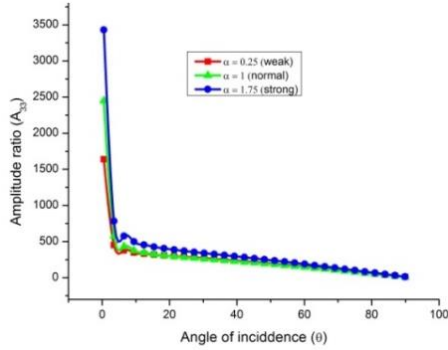


Fig. 22 Variation of amplitude ratio of A_{33} with respect of angle of incidence θ

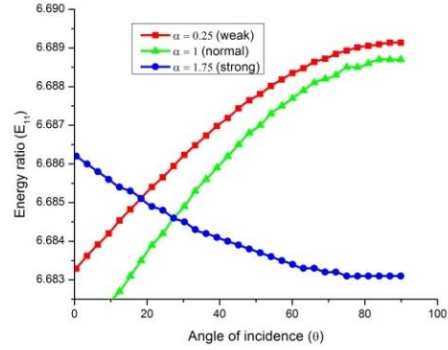


Fig. 23 Variation of energy ratio E_{11} with respect of angle of incidence θ

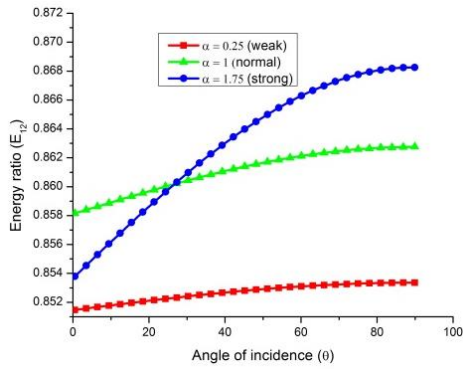


Fig. 24 Variation of energy ratio E_{12} with respect of angle of incidence θ

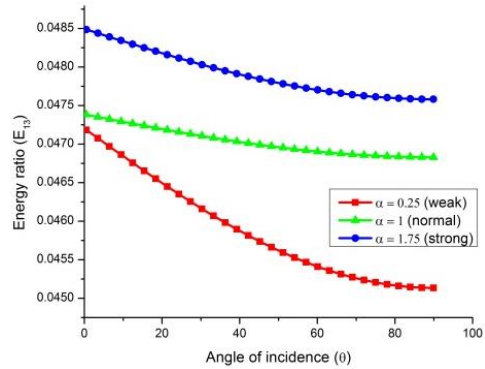


Fig. 25 Variation of energy ratio E_{13} with respect of angle of incidence θ

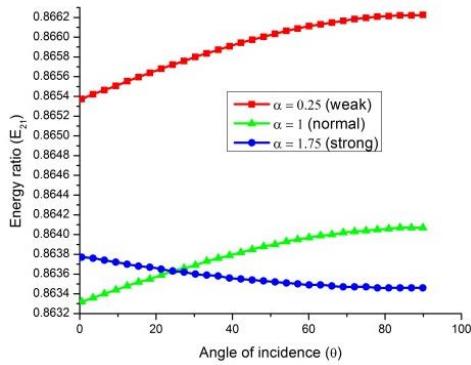


Fig. 26 Variation of energy ratio E_{21} with respect of angle of incidence θ

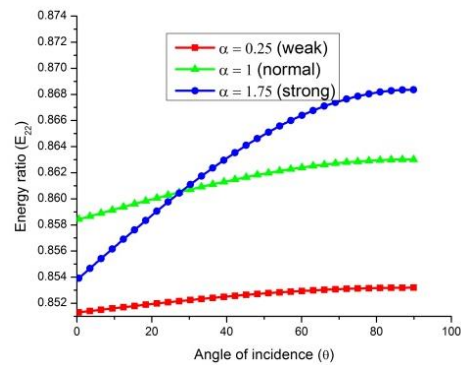


Fig. 27 Variation of energy ratio E_{22} with respect of angle of incidence θ

increases in all the three cases in the whole range with difference in their magnitude values. From the Fig. 28, we see that the value of energy ratio E_{23} declines linearly corresponding to all values of $\alpha=0.25, 1, 1.75$ respectively throughout.

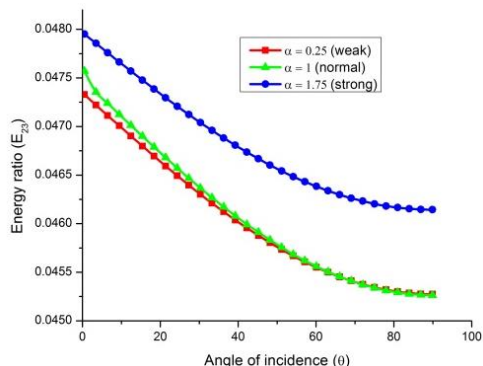


Fig. 28 Variation of energy ratio E_{23} with respect of angle of incidence θ

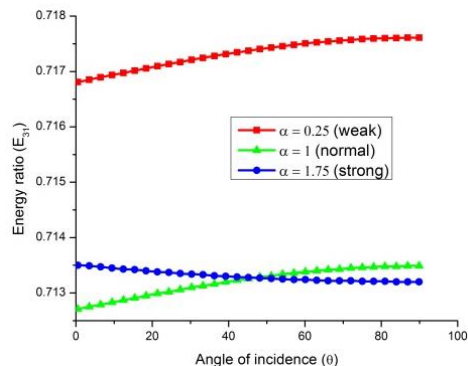


Fig. 29 Variation of energy ratio E_{31} with respect of angle of incidence θ

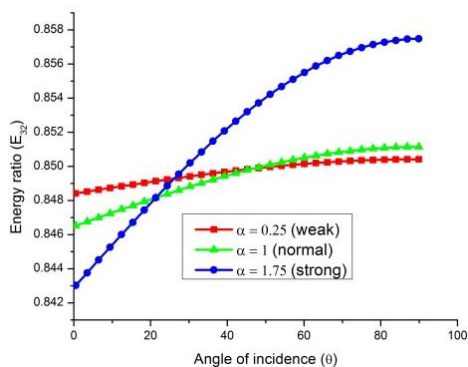


Fig. 30 Variation of energy ratio E_{32} with respect of angle of incidence θ

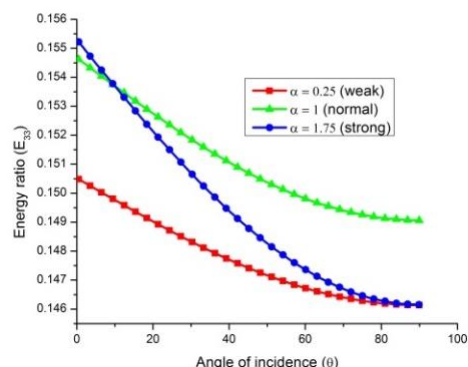


Fig. 31 Variation of energy ratio E_{33} with respect of angle of incidence θ

13.3 Incident QT-wave

Figs. 29-31 depicts the variations of energy ratios E_{31}, E_{32}, E_{33} of QT-wave with respect to angle of incidence θ . From Fig. 29, it can be observed that the value of energy ratio increases smoothly for $\alpha = 0.25, 1$ in the whole range whereas for $\alpha = 1.75$ in the whole range of angle of incidence θ the trends are opposite. Fig 30 describes the behaviour of energy ratio E_{32} with respect to angle of incidence θ . We noticed that its value increases steadily for $\alpha = 0.25, 1$ respectively. For $\alpha = 1.75$ there is a sharp increase in its value and attains its peak at $\theta = 90^\circ$. The variation of E_{33} has shown in Fig. 31. We see that the behaviour is just opposite in this case i.e., decreases for all values of fractional parameter.

14. Conclusions

In the present investigation, the nature of plane harmonic waves in a magneto-thermoelastic orthotropic media with combined effect of rotation and two-temperature in the context of fractional order heat transfer in frequency domain has been noticed. We examined the impact of

fractional order parameter on all the field components with respect to frequency. From the graphical results, we conclude that the phase velocities of all the three waves oscillate in the initial range $0 < \xi < 10$ then increases sharply in the whole range of frequency. It is observed that the value of attenuation coefficients for the QL-waves declines while for QTS and QT-waves it increases near the boundary surface afterwards it decreases monotonically with different magnitudes. Further the change in the specific loss for the QL, QTS and QT waves oscillates in the starting range then remains constant as the angle of incidence increases. The value of penetration depth increases linearly for QL-waves. For QTS and QT-waves it declines initially then increases monotonically and approaches to its maximum value as the angle of incidence increases. The variations in the amplitude ratios for all the three waves show similar behaviour i.e., its value declines throughout with different magnitudes. Further, we observed that the value of energy ratios is either increasing or decreasing monotonically with in the whole range of angle of incidence. Collectively we can say that the fractional parameter changes the magnitude of waves. Further, these wave signals not only give the information about the internal layer of the earth but also helpful in exploration of new materials such as crystals and minerals etc.

References

- Abbas, I.A. and Marin, M. (2017), "Analytical solution of thermoelastic interaction in a half-space by pulsed laser heating", *Physica E: Low Dimens. Syst. Nanostr.*, **87**, 254-260. <http://doi.org/10.2016/j.physe.2016.10.048>.
- Abbas, I.A., Saeed, T. and Alhothuali, M. (2021), "Hyperbolic two-temperature photo-thermal interaction in a semiconductor medium with a cylindrical cavity", *Silicon*, **13**(2), 1871-1878. <http://doi.org/10.1007/s-12633-020-00570-7>.
- Abd-Alla, A.N. and Abbas, I.A. (2002), "A problem of generalized magneto-thermoelasticity for an infinitely long, perfectly conducting cylinder", *J. Therm. Stress.*, **25**(11), 1009-1025. <https://doi.org/10.1080/01495730290074612>.
- Abouelregal, A.E., Elhagary, M.A., Soleiman, A. and Khalil, K.M. (2020), "Generalized thermoelastic-diffusion model with higher-order fractional time derivatives and four-phase-lags", *Mech. Bas. Des. Struct. Mach.*, **50**(3), 897-914. <http://doi.org/10.1080/15397734.2020.1730189>.
- Bakoura, A., Djedid, I.K., Bourada, F., Bousahla, A.A., Mahmoud, S.R., Tounsi, A., ... & Alnujaie, A. (2022), "A mechanical behavior of composite plates using a simple three variable refined plate theory", *Struct. Eng. Mech.*, **83**(5), 617-625. <https://doi.org/10.12989/sem.2022.83.5.617>.
- Bhatti, M.M., Sait, S.M., Ellahi, R., Sheremet, M.A. and Oztop, H.F. (2022), "Thermal analysis of entropy generation of magnetic eyring-powell nanofluid with viscous dissipation in a wavy asymmetric channel", *Int. J. Numer. Meth. Heat Fluid Flow*, <https://doi.org/10.1108/HFF-07-2022-0420>.
- Bhatti, M.M., Shahid, A., Sarris, L.E. and Beg, O.A. (2023), "Spectral relaxation computation of Maxwell fluid flow from a stretching surface with quadratic convection and non-Fourier heat flux using Lie symmetry transformations", *Int. J. Modern Phys. B*, **37**(9), 2350082. <https://doi.org/10.1142/S0217979223500820>.
- Biswas, S. and Abo-Dahab, S.M. (2018), "Effect of phase lags on Rayleigh wave propagation in initially stressed magneto-thermoelastic orthotropic medium", *Appl. Math. Model.*, **59**, 713-727. <https://doi.org/10.1016/j.apm.2018.02.025>.
- Borejko, P. (1996), "Reflection and transmission coefficients for three dimensional plane waves in elastic media", *Wave Motion*, **24**(4), 371-393. [https://doi.org/10.1016/S0165-2125\(96\)00026-1](https://doi.org/10.1016/S0165-2125(96)00026-1)
- Bot, I.K., Bousahla, A.A., Zemri, A., Sekkal, M., Kaci, A., Bourada, F., ... & Mahmoud, SR. (2022), "Effects of Pasternak foundation on the bending behavior of FG porous plates in hygrothermal environment", *Steel Compos. Struct.*, **43**(6), 821-837. <https://doi.org/10.12989/scs.2022.43.6.821>.

- Bouafia, K., Selim, M.M., Bourada, F., Bousahla, A.A., Bourada, M., Tounsi, A., ... & Tounsi, A. (2021), "Bending and free vibration characteristics of various compositions of FG plates on elastic foundation via quasi 3D HSDT model", *Steel Compos. Struct.*, **41**(4), 487-503. <https://doi.org/10.12989/scs.2021.41.4.487>.
- Chen, P.J. and Gurtin, E.M. (1968), "On a theory of heat conduction involving two temperatures", *Zeitschrift für Angewandte Mathematik und Physik*, **19**(4), 614-627.
- Chen, P.J., Gurtin, E.M. and Williams, O.W. (1969), "On the thermodynamics of non-simple elastic materials with two temperatures", *Zeitschrift für angewandte Mathematik und Physik*, **20**(1), 107-112.
- Chen, P.J., Gurtin, M.E. and Williams, W.O. (1968), "A note on non-simple heat conduction", *Zeitschrift für Angewandte Mathematik und Physik ZAMP*, **19**(4), 969-970.
- Das, P. and Kanoria, M. (2014), "Study of finite thermal waves in a magneto-thermoelastic rotating medium", *J. Therm. Stress.*, **37**(4), 405-428. <https://doi.org/10.1080/01495739.2013.870847>.
- Deswal, S. and Kalkal, K.K. (2014), "Plane waves in a fractional order micropolar magneto-thermoelastic half-space", *Wave Motion*, **51**(1), 100-113. <http://doi.org/10.1016/j.wavemoti.2013.06.009>.
- Djilali, N., Bousahla, A.A., Kaci, A., Selim, M.M., Bourada, F., Tounsi, A., ... & Mahmoud, S.R. (2022), "Large cylindrical deflection analysis of FG carbon nanotube-reinforced plates in thermal environment using a simple integral HSDT", *Steel Compos. Struct.*, **42**(6), 779-789. <https://doi.org/10.12989/scs.2022.42.6.779>.
- Ezzat, M.A. (2020), "Fractional thermo-viscoelastic response of biological tissue with variable thermal material properties", *J. Therm. Stress.*, **43**(9), 1120-1137. <http://doi.org/10.1080/01495739.2020.1770643>.
- Hachemi, H., Bousahla, A.A., Kaci, A., Bourada, F., Tounsi, A., Benrahou, K.H., ... & Mahmoud, S.R. (2021), "Bending analysis of functionally graded plates using a new refined quasi-3D shear deformation theory and the concept of the neutral surface position", *Steel Compos. Struct.*, **39**(1), 51-64. <http://doi.org/10.12989/scs.2021.39.1.051>.
- Hebali, H., Chikh, A., Bousahla, A.A., Bourada, F., Tounsi, A., Benrahou, K.H., ... & Tounsi, A. (2022), "Effect of the variable visco-Pasternak foundations on the bending and dynamic behaviors of FG plates using integral HSDT model", *Geomech. Eng.*, **28**(1), 49-64. <https://doi.org/10.12989/gae.2022.28.1.049>.
- Hobiny, A.D. and Abbas, I.A. (2017), "A study on photothermal waves in an unbounded semiconductor medium with cylindrical cavity", *Mech. Time Depend. Mater.*, **21**(1), 61-72. <https://doi.org/10.1007/s11043-016-9318-8>.
- Kaur, R., Lata, P. and Singh, K. (2021), "Reflection of plane harmonic wave in rotating media with fractional order heat transfer and two temperature", *Part. Diff. Equ. Math.*, **4**, 100049. <https://doi.org/10.1016/j.pdiff.2021.100049>.
- Kaushal, S., Sharma, N. and Kumar, R. (2010), "Propagation of waves in generalized thermoelastic continua with two-temperature", *Int. J. Appl. Mech. Eng.*, **15**(4), 1111-1127.
- Khamis, A.K., Abdel Allah Nasr, A.M., EL-Bary, A.A. and Atef, H.M. (2021), "Effect of modified ohm's and Fourier's laws on magneto thermo-viscoelastic waves with Green-Naghdi theory in a homogeneous isotropic hollow cylinder", *Int. J. Adv. Appl Sci.*, **8**(6), 40-47. <http://doi.org/10.18333/ijaas.2021.06.005>.
- Kouider, D., Kaci, A., Selim, M.M., Bousahla, A.A., Bourada, F., Tounsi, A., ... & Hussain, M. (2021), "An original four-variable quasi-3D shear deformation theory for the static and free vibration analysis of new type of sandwich plates with both FG face sheets and FGM hard core", *Steel Compos. Struct.*, **41**(2), 167-191. <http://doi.org/10.12989/scs.2021.41.2.167>.
- Kumar, R. and Chawla, V. (2014), "General solution and fundamental solution for two-dimensional problem in orthotropic thermoelastic media with voids", *Theor. Appl. Mech.*, **41**(4), 247-265. <http://doi.org/10.2298/TAM1404247>.
- Kumar, R. and Gupta, V. (2013), "Plane wave propagation in an anisotropic thermoelastic medium with fractional order derivative and void", *J. Thermoelast.*, **1**(1), 21-34.
- Lata, P. and Himanshi. (2021a), "Orthotropic magneto-thermoelastic solid with multi-dual-phase-lag model and hall current", *Couple. Syst. Mech.*, **10**(2), 103-121. <http://doi.org/10.12989/csm.2021.10.2.103>
- Lata, P. and Himanshi. (2021b), "Orthotropic magneto-thermoelastic solid with higher order dual-phase-lag model in frequency domain", *Struct. Eng. Mech.*, **77**(3), 315-327.

- <http://doi.org/10.12289/sem.2021.77.3.315>.
- Lata, P. and Himanshi. (2021c), "Stoneley wave propagation in an orthotropic thermoelastic media with fractional order theory", *Compos. Mater. Eng.*, **3**(1), 57-70. <http://doi.org/10.12989/cme.2021.3.1.057>.
- Lata, P., Kumar, R. and Sharma, N. (2016), "Plane waves in an anisotropic thermoelastic", *Steel Compos. Struct.*, **22**(3), 567-587. <http://doi.org/10.12989/scs.2016.22.3.567>.
- Marin, M., Codarcea, L. and Chirila, A. (2017), "Qualitative results on mixed problem of micropolar bodies with microtemperatures", *Appl. Appl. Math.*, **12**(2), 776-789.
- Marin, M., Chirila, A. and Othman, M.I.A. (2019), "An extension of Dafermos's results for bodies with a dipolar structure", *Appl. Math. Comput.*, **361**, 680-688. <https://doi.org/10.1016/j.amc.2019.06.024>.
- Merazka et al. (2021), "Hygro-thermo-mechanical bending response of FG plates resting on elastic foundations", *Steel Compos. Struct.*, **39**(5), 631-643. <http://doi.org/10.12989/scs.2021.39.5.631>.
- Othman, M.I.A., Khan, A., Jahangir, R. and Jahangir, A. (2019b), "Analysis on plane waves through magneto-thermoelastic microstretch rotating medium with temperature dependent elastic properties", *Appl. Math. Model.*, **65**, 535-548. <http://doi.org/10.1016/j.apm.2018.08.032>.
- Othman, M.I.A., Said, S. and Marin, M. (2019a), "A novel model of plane waves of two-temperature fiber-reinforced thermoelastic medium under the effect of gravity with three-phase-lag model", *Int. J. Numer. Meth. Heat Fluid Flow*, **29**(12), 4788-4806. <http://doi.org/10.1108/HFF-04-2019-0359>.
- Sharma, K. and Bhargava, R.R. (2014), "Propagation of thermoelastic plane waves at an imperfect boundary of thermal conducting viscous liquid/generalized thermoelastic solid", *Afrika Mathematica*, **25**(1), 81-102. <https://doi.org/10.1007/s13370-012-0099-1>.
- Sharma, K. and Kumar, P. (2013), "Propagation of plane waves and fundamental solution in thermo-viscoelastic medium with voids", *J. Therm. Stress.*, **36**(2), 94-111. <https://doi.org/10.1080/01495739.2012.720545>.
- Singh, B. and Singh, A. (2021), "Reflection of plane waves from the boundary of a thermo-magneto-electroelastic solid half space", *Couple. Syst. Mech.*, **10**(2), 143-159. <http://doi.org/10.12989/csm.2021.10.2.143>.
- Sinha, S.B. and Elsibai, K.A. (1997), "Reflection and refraction of thermoelastic waves at an interface of two semi-infinite media with two relaxation times", *J. Therm. Stress.*, **20**(2), 129-145. <https://doi.org/10.1080/01495739708956095>.
- Tahir, S.I., Tounsi, A., Chikh, A., Al-Osta, M.A., Al-Dulaijan, S.U. and Al-Zahrani, M.M. (2022), "The effect of three-variable viscoelastic foundation on the wave propagation in functionally graded sandwich plates via a simple quasi-3D HSDT", *Steel Compos. Struct.*, **42**(4), 501-511. <https://doi.org/10.12989/scs.2022.42.4.501>.
- Vinh, P.V. and Tounsi, A. (2022), "Free vibration analysis of functionally graded doubly curved nanoshells using nonlocal first-order shear deformation theory with variable nonlocal parameters", *Thin Wall. Struct.*, **174**, 109084. <https://doi.org/10.1016/j.tws.2022.109084>.
- Vinh, P.V., Chinh, N.V. and Tounsi, A. (2022), "Static bending and buckling analysis of bi-directional functionally graded porous plates using an improved first-order shear deformation theory and FEM", *Eur. J. Mech.*, **96**, 104743. <https://doi.org/10.1016/j.euromechsol.2022.104743>.
- Youssef, H.M. (2006), "Theory of two temperature generalized thermoelasticity", *IMA J. Appl. Math.*, **71**(3), 383-390. <http://doi.org/10.1093/imamat/hxh101>.
- Zakaria, M. (2014), "Effect of hall current on generalized Magneto-thermoelasticity micropolar solid subject to ramp type heating", *Appl. Mech.*, **50**(1), 92-104. <https://doi.org/10.1007/s10778-014-0615-0>.
- Zhang, L., Bhatti, M.M., Marin, M. and Mekheimer, K.S. (2020), "Entropy analysis on the blood flow through anisotropically tapered arteries filled with magnetic zinc-oxide (ZnO) nanoparticles", *Entropy*, **22**(10), 1070. <http://doi.org/10.3390/e22101070>.